© 2019. Published by The Company of Biologists Ltd | Development (2019) 146, dev178145. doi:10.1242/dev.178145

RESEARCH REPORT

Nkx2-5 defines a subpopulation of pacemaker cells and is essential for the physiological function of the sinoatrial node in mice

Hua Li[1,2], Dainan Li[2], Yuzhi Wang[2], Zhen Huang[1], Jue Xu[2,3], Tianfang Yang[2], Linyan Wang[2,4], Qinghuang Tang[2], Chen-Leng Cai[5], Hai Huang[2], Yanding Zhang[1] and YiPing Chen[2,*]

ABSTRACT

The sinoatrial node (SAN), the primary cardiac pacemaker, consists of a head domain and a junction/tail domain that exhibit different functional properties. However, the underlying molecular mechanism defining these two pacemaker domains remains elusive. Nkx2-5 is a key transcription factor essential for the formation of the working myocardium, but it was generally thought to be detrimental to SAN development. However, *Nkx2-5* is expressed in the developing SAN junction, suggesting a role for *Nkx2-5* in SAN junction development and function. In this study, we present unambiguous evidence that SAN junction cells exhibit unique action potential configurations intermediate to those manifested by the SAN head and the surrounding atrial cells, suggesting a specific role for the junction cells in impulse generation and in SAN-atrial exit conduction. Single-cell RNA-seq analyses support this concept. Although *Nkx2-5* inactivation in the SAN junction did not cause a malformed SAN at birth, the mutant mice manifested sinus node dysfunction. Thus, *Nkx2-5* defines a population of pacemaker cells in the transitional zone. Despite *Nkx2-5* being dispensable for SAN morphogenesis during embryogenesis, its deletion hampers atrial activation by the pacemaker.

KEY WORDS: Nkx2-5, Shox2, Sinoatrial node, Cardiac conduction system, Sinus node dysfunction

INTRODUCTION

The rhythmic heartbeats in mammals are regulated by a steady pace of electrical impulses generated by the sinoatrial node (SAN), functionally known as the primary cardiac pacemaker (Christoffels et al., 2010; Moorman et al., 1998; Ye et al., 2015a). Anatomically, the SAN is a structurally heterogeneous tissue with a densely packed head domain that extends superiorly and wraps around the right superior vena cava (RSVC), and a loosely packed junction/tail region that extends inferiorly towards the inferior vena cava (IVC) (Boyett et al., 2000; Liu et al., 2007; Opthof, 1988). Interestingly, the SAN junction can maintain pacemaker function even in the presence of a severe hypoplastic SAN head, as shown in *Tbx18* mutants (Wiese et al., 2009). In contrast, mice lacking *Shox2* in the SAN junction manifest severe sinus node dysfunction associated with a virtual absence of the SAN junction, despite a normal SAN head (Ye et al., 2015b). This observation demonstrates an essential role for the SAN junction in normal pacemaking function. However, whether more than one population of pacemaking cells exist in the SAN remained an unanswered question. Additionally, the mechanism and molecular basis responsible for the distinct function of the SAN head and junction are also unknown.

SAN development has been studied extensively. Gene expression and genetic studies in mice have revealed a complex genetic network involving many genes, including *Hcn4*, *Tbx3*, *Tbx5*, *Tbx18*, *Isl1* and *Shox2* (Munshi, 2012). Among them, *Shox2*, *Tbx3*, *Isl1* and *Hcn4* are expressed in the entire developing SAN, with *Hcn4* being regarded as a functional marker of the SAN (Moosmang et al., 2001; Santoro and Tibbs, 1999). *Nkx2-5*, one of the earliest cardiac-specific markers, plays an essential role in heart formation (Lints et al., 1993; Moses et al., 2001). Previously, *Nkx2-5* was thought to be excluded from the developing SAN and to be essential for establishing a strict boundary between the SAN domain and the surrounding atrial myocardium by inhibiting *Tbx3* and *Hcn4*, but activating *Cx40* (*Gja5*) expression (Christoffels et al., 2006; Espinoza-Lewis et al., 2011; Kasahara et al., 1998; Mommersteeg et al., 2007). Despite repression of *Nkx2-5* by *Tbx3* and *Shox2* in the SAN head region (Blaschke et al., 2007; Espinoza-Lewis et al., 2009; Wu et al., 2014), *Nkx2-5* expression was nevertheless detected in the developing SAN junction (Liang et al., 2013; Wiese et al., 2009; Ye et al., 2015b). Our recent studies demonstrated that, in the developing SAN junction, Shox2 functions to inhibit the transcriptional output of Nkx2-5 through a Shox2-Nkx2-5 antagonistic mechanism (Ye et al., 2015b). However, whether *Nkx2-5* is essential for the development of the SAN junction and SAN function is completely unknown.

RESULTS AND DISCUSSION

Patch-clamp recording identifies two distinct populations of pacemaking cells in the developing SAN

While several molecular markers, including *Hcn4*, *Shox2*, *Isl1* and *Tbx3*, are expressed in the entire developing SAN, *Tbx18* expression is restricted to the SAN head, and *Nkx2-5* expression is found in the SAN junction from early embryonic stage to adulthood, indicating the existence of two genetically distinct domains in the SAN (Wiese et al., 2009; Munshi, 2012; Ye et al., 2015a,b; Fig. 1A-C′). Although genetic studies have demonstrated different requirements of these two domains for pacemaking function, the exact cell

[1]Southern Center for Biomedical Research and Fujian Key Laboratory of Developmental and Neural Biology, College of Life Sciences, Fujian Normal University, Fuzhou, Fujian Province 350108, PR China. [2]Department of Cell and Molecular Biology, Tulane University, New Orleans, LA 70118, USA. [3]West China School of Public Health and West China Fourth Hospital, Sichuan University, Chengdu, Sichuan Province 610041, PR China. [4]State Key Laboratory of Oral Diseases, National Clinical Research Center for Oral Diseases, Department of Preventive Dentistry, West China Hospital of Stomatology, Sichuan University, Chengdu, Sichuan Province 610041, PR China. [5]Department of Pediatrics, Indiana University School of Medicine, Indianapolis, IN 46202, USA.

*Author for correspondence (ychen@tulane.edu)

C.-L.C., 0000-0002-8628-7713

Received 18 March 2019; Accepted 4 July 2019

Development (2019) 146, dev178145. doi:10.1242/dev.178145

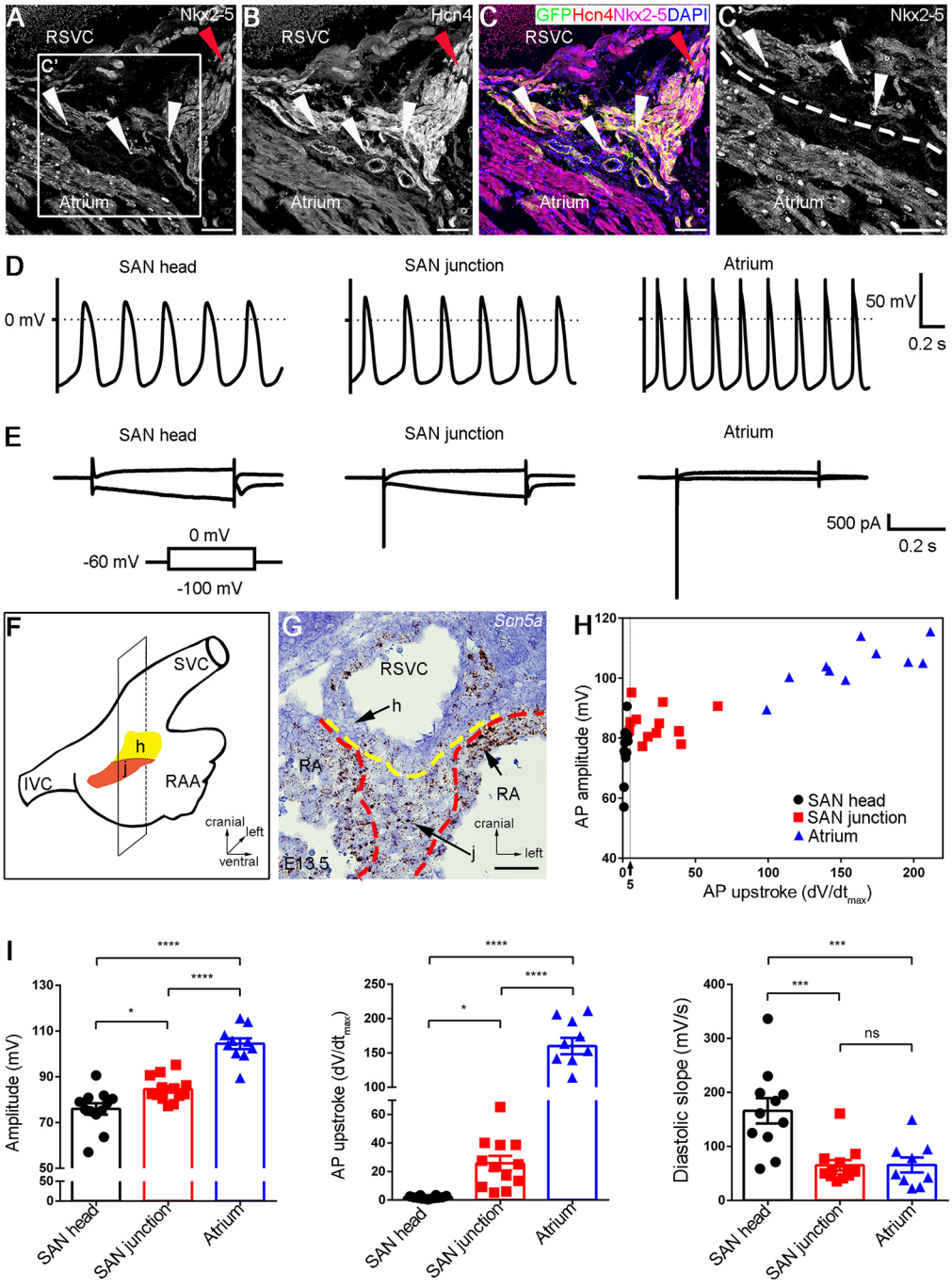

Fig. 1. AP recordings identify two distinct types of pacemaking cells in the SAN. (A-C,C′) Co-immunofluorescent staining shows the persistent expressions of Nkx2-5 and Hcn4 in the SAN junction of *Shox2*$^{Cre/+}$;*R26R*^{mTmG} mice at adulthood. Red arrowheads indicate the SAN head; white arrowheads indicate the Nkx2-5^{+} cells in the SAN junction. (D) Sample traces of spontaneous action potentials show typical firing configurations of cells from the SAN head, SAN junction and atrium. (E) Typical examples of the current response in the SAN head, SAN junction and atrium cells upon 0.5 s voltage step from holding the potential of –60 mV to –100 mV or 0 mV. (F) Schematic overview of the section plane on the SAN shown in G. (G) *In situ* hybridization shows *Scn5a* expression in the SAN junction and atrial tissue. The expression level in the SAN junction is lower than that in the atrial cells. (H) A two-dimensional diagram shows the AP amplitude and AP upstroke for each type of cell. (I) Summary graphs of the AP amplitude, AP upstroke and diastolic slope in each group. Data are mean ±s.e.m. ns, non-significant; *P<0.05; ***P<0.001; ****P<0.0001. h, SAN head; j, SAN junction; RA, right atrium; IVC, inferior vena cava; RAA, right atrial appendage; SVC, superior vena cava. Scale bars: 50 µm.

identity in these two distinct SAN regions has not been studied, likely due to difficulties in determining the precise isolation of cells from each domain. We took advantage of several unique genetically modified mouse lines that can precisely define the SAN head and junction domains. We compounded these alleles to generate mice carrying *Nkx2-5*$^{Cre/+}$;*Shox2*$^{HA-DsRed}$;*R26R*^{YFP} alleles. In these mice, the entire SAN is labeled by DsRed expressed from the *Shox2*$^{HA-DsRed}$ allele (Ye et al., 2015b), while the junction domain is marked by both DsRed and YFP that is activated by the *Nkx2-5*^{Cre} allele. As a result, the junction cells (DsRed^{+}/YFP^{+}) are distinguishable from the surrounding atrial (YFP^{+}) and SAN head cells (DsRed^{+}) (Fig. S1).

To understand the developmental status of the electrophysiological properties of a SAN cell, we developed an *exo utero* electrocardiography (ECG) protocol whereby an ECG recording is conducted on embryos via the placenta to the uterus attachment within the female abdominal cavity. We performed *exo utero* ECG on wild-type embryos from embryonic day 12.5 (E12.5) to E16.5 and found that the P waves, which accurately reflect atrial depolarization, became detectable at E12.5, and appeared typically from E13.5 onwards (Fig. S2), consistent with a previous report that SAN cells begin to exhibit typical action potential (AP) configurations of pacemaking activity at E12.5 (van Eif et al., 2019). Therefore, we isolated the SAN and adjacent atrial tissues from E13.5 *Nkx2.5*$^{Cre/+}$;*Shox2*$^{HA-DsRed}$;*R26R*^{YFP} embryos. Single cells were dissociated from the tissues and plated in culture. Patch-clamp recordings were performed on cultured cells from the SAN head and junction, as well as the atrial tissues, based on

Development (2019) 146, dev178145. doi:10.1242/dev.178145

corresponding fluorescent markers. The AP properties of the SAN head cells and atrial cells (Fig. 1) exhibited typical configurations characterized previously for pacemaking and atrial cells (Sun et al., 2015; van Eif et al., 2019; Ye et al., 2015b; Zhang et al., 2002). However, the SAN junction cells presented unique AP configurations that were intermediate to those produced by the SAN head and atrial cells (Fig. 1). The AP amplitude in the SAN junction cells was larger in comparison with the SAN head cells, but smaller than that in the atrial cells (Fig. 1). The AP upstroke, which is the maximal rate of the rising, was faster in the SAN junction cells than that in the SAN head cells, but slower in comparison with the atrial cells (Fig. 1). The AP amplitude and the AP upstroke from each cell type are summarized in Fig. 1H, which demonstrates that the SAN junction cells have characteristics of both the SAN head and atrial cells. Statistical analysis of the AP configurations from these three types of cells showed significant differences between each of them (Fig. 1I and Fig. S3), indicating that the SAN cells are electrically heterogeneous. Moreover, compared with the *Nkx2-5*$^{-}$ head and the atrial cells, the *Nkx2-5*$^{+}$ SAN junction cells showed a distinct electrophysiological property manifested by both the hyperpolarization-activated HCN current that shows only in the SAN head cells and the depolarization-activated fast sodium current that is seen in the atrial cells (Fig. 1E,G). Previous studies have shown that the electrical coupling during propagation of APs from the SAN to the atrium creates transitional AP shapes in the cells adjacent to the border zone of these two different cell types (Joyner and Van Capelle, 1986; Verheijck et al., 1998; Zhang et al., 2001). Thus, the SAN junction cells show combinatory electrophysiological properties of the SAN head and atrial cells. This domain appears to act as a transitional zone in which the spontaneous firing arising from the HCN current elicits the activity generated by the fast sodium channel, thus playing a role in both impulse generation and SAN-atrial exit conduction.

scRNA-seq reveals distinct gene expression profiles underlying the cellular heterogeneity of the SAN

The functional heterogeneity of a cell population is often a reflection of cellular heterogeneity (Tan et al., 2013). Recently, single-cell RNA-sequencing (scRNA-seq) has become a powerful tool for profiling cell-to-cell variability on a transcriptomic scale. We conducted an unbiased survey of the cellular diversity in the SAN, with the surrounding atrial cells as a reference control. The SAN domain, which is highlighted by GFP, was isolated with adjacent atrial tissue from E13.5 *Shox2*$^{Cre/+}$;*R26R*^{mTmG} mice and subjected to scRNA-seq. As quality control of the duplicate samples was mostly coincident (Fig. S4C), we chose one of them for deeper sequencing and further analysis. A total of 3770 individual cells from the SAN and atrium were profiled. After unbiased analysis, 2005 cells were acquired and subjected to significant principal components analysis, resulting in eight distinct clusters, including cardiomyocytes (CM), mesenchymal cells (MC), vascular smooth muscle (VSM), endothelial cells (ECs), epicardial cells (EPIs) and macrophages (Chasseigneaux et al., 2018; DeLaughter et al., 2016; Khazen et al., 2005; Lee et al., 2017; Li et al., 2016; Souders et al., 2009; Tarnawski et al., 2015; Vanlandewijck et al., 2018; Fig. 2B). The clustering results were visualized through the non-linear dimensional reduction algorithm, t-distributed stochastic neighbor embedding(tSNE) (Maaten and Hinton, 2008; Macosko et al., 2015). Because *Hcn4*, *Gja5*, *Nppa*, *Nkx2-5* and *Tnnt2* genes were all present within the CM cluster (Fig. S4), the 450 cells in the CM cluster were then used for further analysis, which further identified four clusters (C0 to C3) (Fig. 2C). Using Seurat (Butler et al., 2018), we found that, among these four clusters, C0 and C1 exhibited expression of several SAN marker genes, including *Isl1*, *Tbx18*, *Hcn4*, *Tbx3*, *Bmp4* and *Smoc2* (Fig. 2D,E, Fig. S4E), as reported previously (Liang et al., 2015; Puskaric et al., 2010; van Eif et al., 2019; Wiese et al., 2009). Thus, C0 and C1 correspond to the SAN cells. C2 showed expression of atrial-specific markers such as *Nppa* and *Itga6* (Lee et al., 2017; Tarnawski et al., 2015; Vedantham et al., 2015), indicating that the C2 population consists of atrial cells. However, in C1, we also found the expression of C2-specific genes, making this group an intermediate between the C0 and C2 populations (Fig. 2D,E). Consistent with the unique AP configurations contributed by both the HCN current and fast sodium current in the SAN junction cells (Fig. 1), C1 cells also expressed *Scn5a*, which is known to be responsible for fast sodium current. Therefore, we determined that C0 corresponds to the SAN head cells and C1 to the SAN junction cells. In addition, the expression of *Gja5* (which encodes Cx40) in C1 would also confer this group of cells with conduction activity (van Weerd and Christoffels, 2016). Although the transcriptome of C3 did not pin-point any specific type of cell, venous valve cells seemed likely. Nevertheless, gene expression profiling supports the existence of a population of SAN cells that exert physiological functions intermediate between the SAN head and atrium in impulse generation and impulse conduction. This is consistent with other data demonstrating that mice lacking the SAN head due to *Tbx18* mutation have a normal beating rhythm, but mice lacking the SAN junction exhibit sinus node dysfunction (Wiese et al., 2009; Ye et al., 2015b).

Nkx2-5 is essential for normal SAN function

As *Nkx2-5* is expressed in the developing SAN junction from E11.5 onwards (Liang et al., 2013; Wiese et al., 2009), we sought to investigate its role in SAN morphogenesis and function. To inactivate *Nkx2-5* in the SAN junction specifically (Fig. 3D-F′), we crossed *Shox2-Cre* knock-in mice that exhibit Cre activity initially in the sinus venosus at E9.0 and later in the developing SAN with *Nkx2-5*$^{F/F}$ mice (Pashmforoush et al., 2004; Sun et al., 2013). These *Shox2*$^{Cre/+}$;*Nkx2-5*$^{F/F}$ mice survived to adulthood without an obvious phenotype. However, although heartbeat rates appeared comparable with controls, surface ECG identified compromised SAN function in adult mutants (2-6 months old) (Fig. 3B,C); manifested sinus node dysfunction included arrhythmia, inverted P wave and sinoatrial exit block (Fig. 3B), which were also found in 1-month-old young mice (data not shown). Detailed ECG measurements are presented in Fig. S5.

To uncover the morphogenetic and molecular changes underlying the sinus node dysfunction in *Shox2*$^{Cre/+}$;*Nkx2-5*$^{F/F}$ mice, we first assessed SAN morphology using the pan-SAN marker Hcn4. We found comparable structures in P0 controls and mutants (Fig. 4A,A′). Three-dimensional (3D) reconstruction of the SAN from E13.5 controls and mutants also showed similar structures (Fig. 4B,B′,L). However, despite similar expression levels and patterns of the SAN markers Tbx3 and Islet1 in the SAN junction of E13.5 controls and mutants, we did observe an elevated level of Hcn4 and a slightly reduced level of Cx40 in the mutants (Fig. 4C-F′). RT-qPCR analyses further confirmed significantly reduced levels of *Nkx2-5*, *Gja5* and *Scn5a* in the SAN of P0 mutants compared with controls (Fig. 4M). Downregulation of *Scn5a* and *Gja5* expression could explain the reduced fast sodium current and conduction activity in the SAN junction, thereby contributing to the sinoatrial exit block. The presence of inverted P wave or diphasic P wave is an indication of the retention of the dominant pacemaking site in the left side of the heart (MacLean et al., 1975). We have

Development (2019) 146, dev178145. doi:10.1242/dev.178145

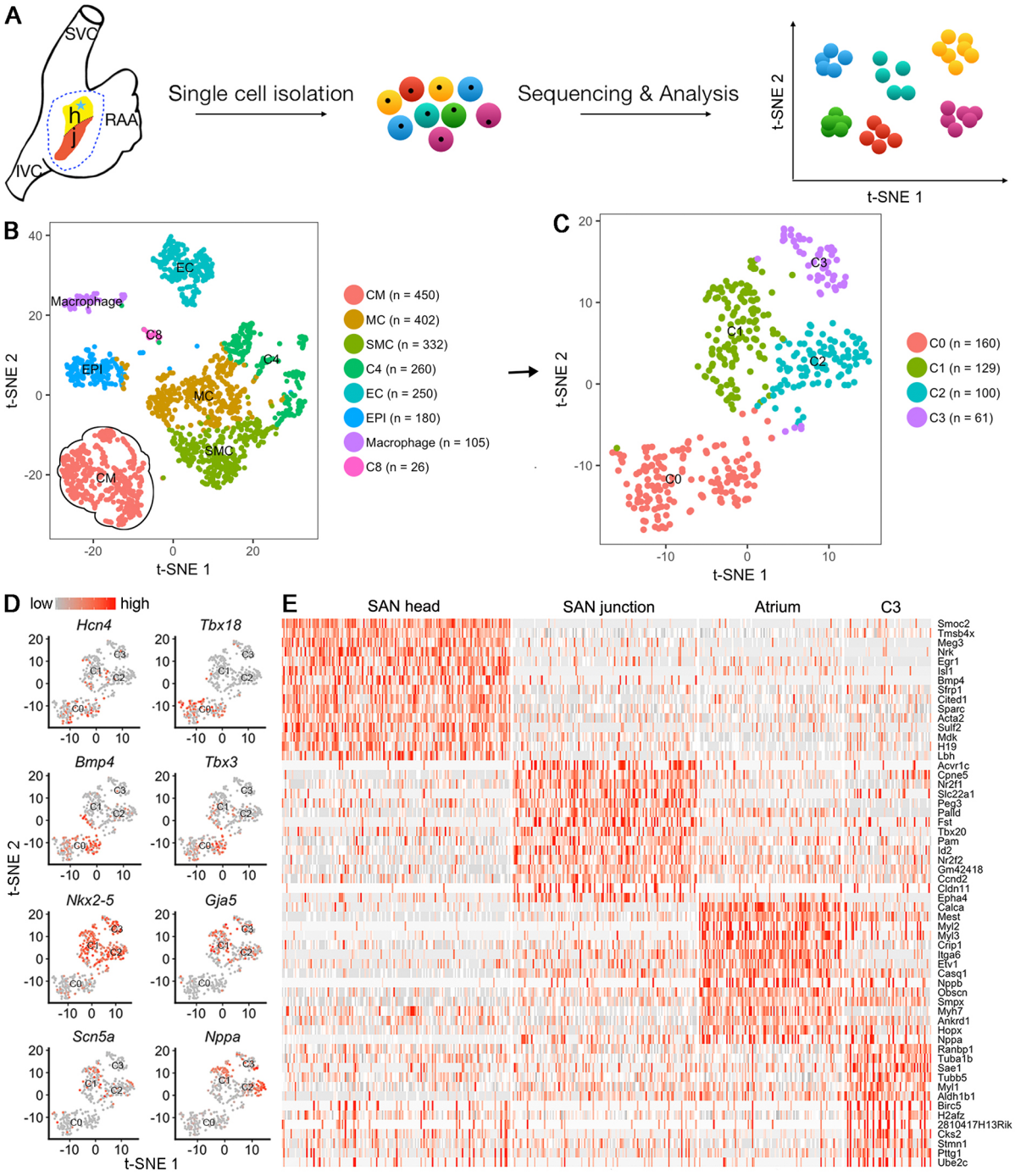

Fig. 2. scRNA-seq of the SAN and atrial cells. (A) Schematic overview of data collection and analysis. (B) tSNE visualization of the eight clusters on the SAN and atrial cells from *Shox2*$^{cre/+}$;*R26R*^{mTmG} mice. (C) A tSNE plot shows four clusters (C0-C3) resulting from iterative clustering of 450 CM cells. (D) The marker gene expression of the SAN head, SAN junction and atrium on the tSNE plot of the four clusters. (E) Heatmap shows the top 15 marker genes for each cluster. CM, cardiomyocyte; EC, endothelial cells; MC, mesenchymal cells; EPI, epicardial cells; IVC, inferior vena cava; RAA, right atrial appendage; SMC, smooth muscle cells; SVC, superior vena cava. C3, C4 and C8 are cluster numbers 3, 4 and 8.

reported previously that *Shox2* and *Nkx2-5* are also co-expressed in the developing pulmonary vein (PV) myocardium and that reduced doses of *Nkx2-5* lead to ectopic Hcn4 expression and reduced Cx40 in the PV myocardium (Ye et al., 2015b). Similar results were observed in the PV myocardium of *Shox2*$^{Cre/+}$;*Nkx2-5*$^{F/F}$ mice (Fig. 4G-J′), which could be responsible for the inverted and diphasic P waves identified by the surface ECG (Fig. 3; Fig. S5). Our results present unambiguous evidence that *Nkx2-5* is dispensable for SAN morphogenesis and differentiation during embryogenesis, but plays an essential role for normal SAN physiological function.

As most SAN-specific markers are present in both the SAN head and junction, but *Nkx2-5* is absent in the SAN head, we wondered whether *Nkx2-5* expression confers the SAN junction cells unique AP configurations. We therefore set out to conduct patch-clamp recordings on the SAN junction cells with deletion of *Nkx2-5*. We

Development (2019) 146, dev178145. doi:10.1242/dev.178145

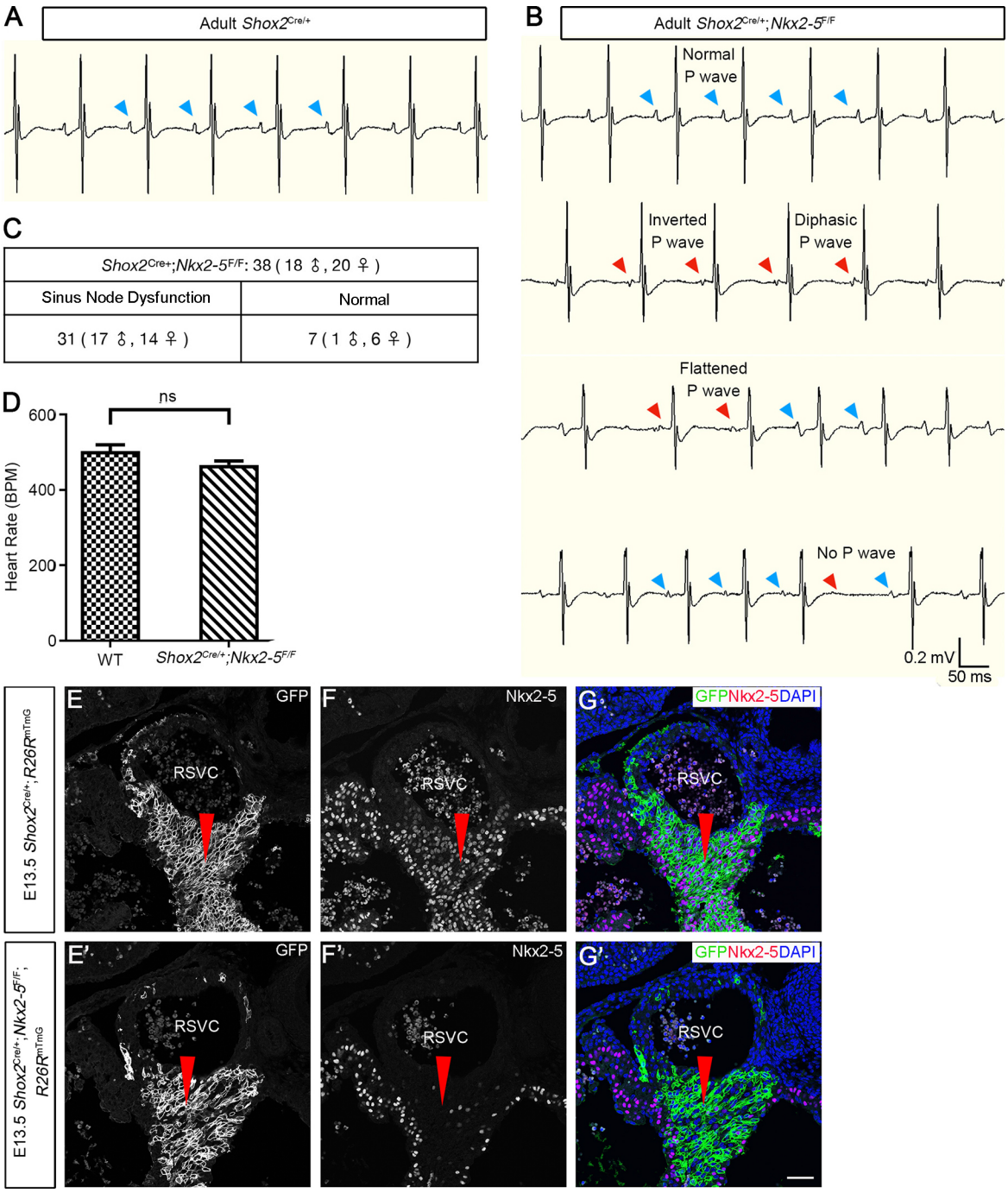

Fig. 3. Deletion of *Nkx2-5* in the SAN junction causes sinus node dysfunction. (A,B) Surface ECG recordings reveal irregular P waves, including an inverted P wave, a diphasic P wave, no P wave and a flattened P wave, in adult *Shox2*$^{Cre/+}$;*Nkx2-5*$^{F/F}$ mice (B, red arrowheads), compared with normal P waves in control mice (A, blue arrowheads). Out of 38 *Shox2*$^{Cre/+}$;*Nkx2-5*$^{F/F}$ mice (18 male and 20 female), 31 (17 male and 14 female) have sinus node dysfunction and 7 (1 male and 6 female) are normal. (C) Heartbeat rates appear comparable in adult *Shox2*$^{Cre/+}$;*Nkx2-5*$^{F/F}$ and control mice. Data are mean ±s.e.m. (D-F′) Immunofluorescence shows an absence of Nkx2-5 in the SAN junction (red arrowheads) of E13.5 *Shox2*$^{Cre/+}$;*Nkx2-5*$^{F/F}$;*R26R*^{mTmG} mice. ns, non-significant; BPM, beats per minute; RSVC, right superior vena cava. Scale bar: 50 µm.

first performed patch-clamp recording on the GFP-positive SAN cells from E13.5 *Shox2*$^{Cre/+}$;*R26R*^{mTmG} and calculated the proportion of head/junction cells in the whole SAN based on their AP configurations, effectively setting a baseline for calibration. In the 17 recorded cells (with 10 expressing typical head AP configurations and seven manifesting typical junction AP configurations), the proportion of head/junction cells (59% vs. 41%) is consistent with the ratio of head/junction cells defined by scRNA-seq (55% versus 45%; Fig. 2C). Thereafter, we randomly recorded 26 GFP-positive cells from the SAN of E13.5 *Shox2*$^{Cre/+}$;*Nkx2-5*$^{F/F}$;*R26R*^{mTmG} mice. Among them, 22 presented head AP patterns and four showed typical junction AP configurations (Fig. S3C). Thus, the majority of the recorded SAN cells (85%) exhibited head AP configurations, suggesting that some of them originated from junction cells. The four cells exhibiting junction AP configurations likely escaped Cre recombination.

Development (2019) 146, dev178145. doi:10.1242/dev.178145

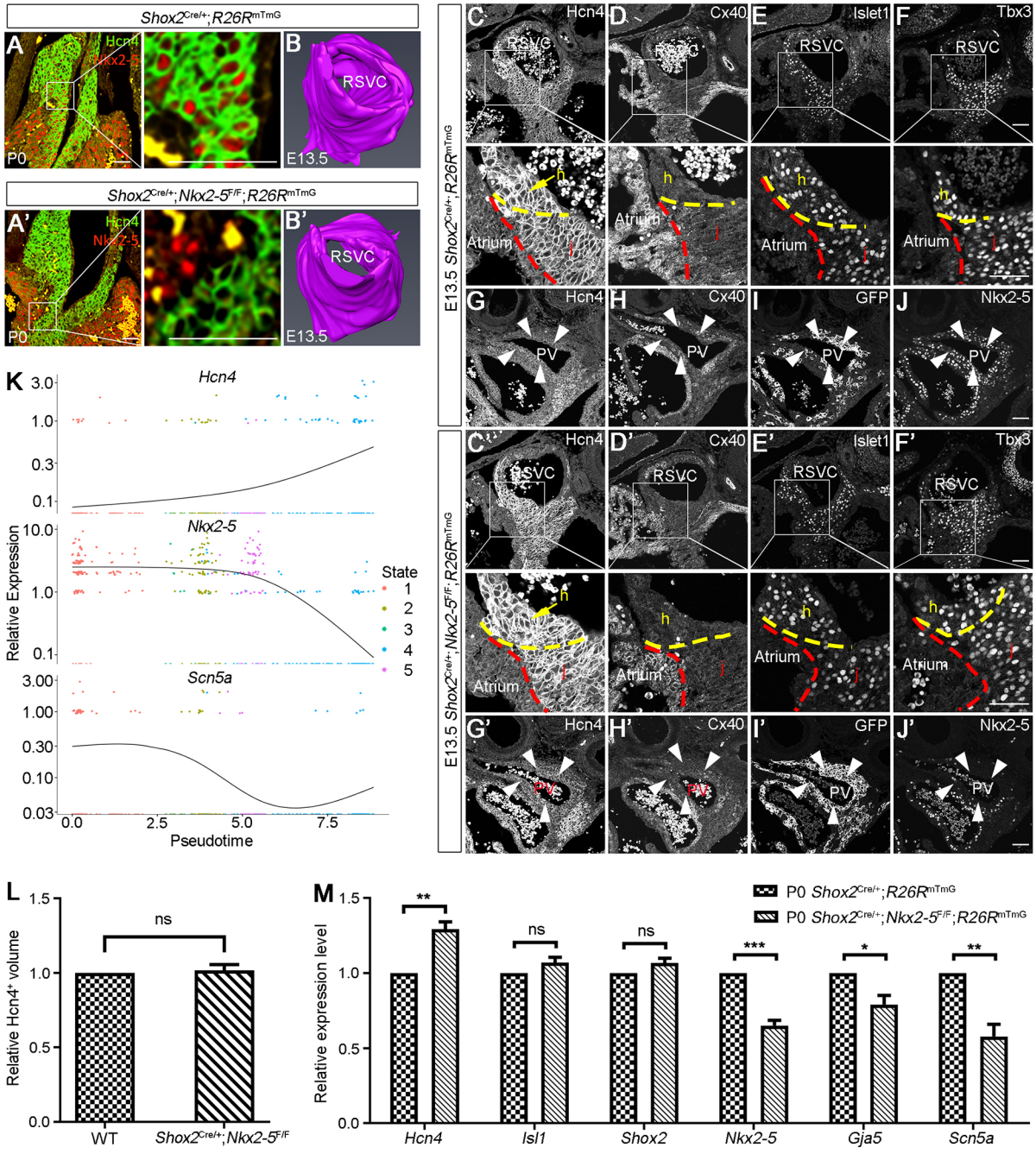

Fig. 4. *Nkx2-5* is dispensable for SAN morphogenesis during embryogenesis. (A,A′) The morphology of the SAN, defined by Hcn4 immunofluorescence, appears comparable between P0 *Shox2*$^{Cre/+}$;*Nkx2-5*$^{F/F}$;*R26R*^{mTmG} and *Shox2*$^{Cre/+}$;*R26R*^{mTmG} mice. (B,B′) 3D reconstruction of the SAN (based on Hcn4 immunostaining) in E13.5 *Shox2*$^{Cre/+}$;*R26R*^{mTmG} and *Shox2*$^{Cre/+}$;*Nkx2-5*$^{F/F}$;*R26R*^{mTmG} mice (*n*=3 for each genotype). (C-F′) Immunofluorescence shows the colocalization of Hcn4, Cx40, Islet1 and Tbx3 in the SAN junction in E13.5 *Shox2*$^{Cre/+}$;*R26R*^{mTmG} and *Shox2*$^{Cre/+}$;*Nkx2-5*$^{F/F}$;*R26R*^{mTmG} mice. Compared with the *Shox2*$^{Cre/+}$;*R26R*^{mTmG} mice (C-F), *Nkx2-5* deletion in the SAN junction of *Shox2*$^{Cre/+}$;*Nkx2-5*$^{F/F}$;*R26R*^{mTmG} mice (C′-F′) caused visible Hcn4 elevation but Cx40 reduction. Intermediate levels of Hcn4 and Cx40 expression are found in the SAN junction compared with the SAN head and surrounding atrial cells in control mice (enlarged images from C,D). Broken lines indicate the boundaries of the atrium, SAN head and SAN junction. (G-J′) Immunofluorescence shows the expression of Nkx2-5, Hcn4 and Cx40 in the PV myocardium of E13.5 *Shox2*$^{Cre/+}$;*R26R*^{mTmG} and *Shox2*$^{Cre/+}$;*Nkx2-5*$^{F/F}$;*R26R*^{mTmG} mice. *Nkx2-5* deletion in *Shox2*$^{Cre/+}$;*Nkx2-5*$^{F/F}$;*R26R*^{mTmG} mice (G′-J′) also resulted in elevated Hcn4 and reduced Cx40 expression compared with the controls (G-J). White arrowheads indicate PV myocardium. (K) The dynamic expression of *Hcn4*, *Scn5a* and *Nkx2-5* along the pseudotime trajectory. (L) Comparison of Hcn4^{+} volume in the SAN of E13.5 *Shox2*$^{Cre/+}$;*Nkx2-5*$^{F/F}$;*R26R*^{mTmG} and *Shox2*$^{Cre/+}$;*R26R*^{mTmG} mice. (M) RT-qPCR assays show downregulated expression of *Nkx2-5*, *Gja5* and *Scn5a*, and upregulated expression of *Hcn4* in the SAN of P0 *Shox2*$^{Cre/+}$;*Nkx2-5*$^{F/F}$;*R26R*^{mTmG} mice. ns, non-significant; *P<0.05; **P<0.01; ***P<0.001. h, SAN head; j, SAN junction; PV, pulmonary vein; RSVC, right superior vena cava. Scale bars: 50 µm.

To further understand the elicited function of *Nkx2-5* in AP configurations, the temporal expression of *Scn5a*, *Hcn4* and *Nkx2-5* in the SAN cells from E13.5 *Shox2*$^{Cre/+}$;*R26R*^{mTmG} mice were reconstructed by pseudotime analysis using Monocle2 (Qiu et al., 2017). We found that expression of *Nkx2-5* and *Scn5a* along the pseudotime trajectory gradually decreased, whereas expression of

Development (2019) 146, dev178145. doi:10.1242/dev.178145

Hcn4 increased (Fig. 4K), strongly suggesting that *Nkx2-5* expression is responsible for the generation of the typical SAN junction AP configurations. In the absence of *Nkx2-5*, the SAN junction cells would stimulate SAN head AP configuration.

Although *Nkx2-5* function in the formation of working myocardium has been well defined, its role in SAN formation is controversial. Although mutations in *Nkx2-5* lead to conduction system disturbances in humans and mice (Benson et al., 1999; Biben et al., 2000; Jay et al., 2004; Schott et al., 1998), *Nkx2-5* was thought to be detrimental to SAN development, at least under overdose conditions (Christoffels et al., 2006; Espinoza-Lewis et al., 2011; Kasahara et al., 1998). Our current studies demonstrate the existence of two distinct domains of the SAN, with the *Nkx2-5*$^{+}$ junction cells exhibiting unique electrophysiological properties and transcriptomic profiles intermediate between the SAN head and the adjacent atrial cells. We also provide convincing evidence that, although it is not required for SAN morphogenesis during embryogenesis, *Nkx2-5* is essential for normal SAN physiological function. Taken together, our studies define two distinct pacemaker cell populations and reveal a novel role for *Nkx2-5* in pacemaking function in the SAN. These results could shed light on the regeneration or directed differentiation of specific pacemaking cell types, and on the development of gene- and cell-based therapies for congenital and acquired cardiac conduction abnormalities.

MATERIALS AND METHODS

Animal models, embryos, histology, immunofluorescence and *in situ* hybridization

The generation and genotyping protocols of *Shox2*^{Cre}, *Shox2*$^{HA\text{-}DsRed}$, *Nkx2.5*^{Cre}, *Nkx2.5*$^{F/F}$, *R26R*^{YFP} and *R26R*^{mTmG} mice have been described previously (Barry et al., 2015; Moses et al., 2001; Muzumdar et al., 2007; Pashmforoush et al., 2004; Sun et al., 2013; Ye et al., 2015b). The animal experiments in this study were approved by the Institutional Animal Care and Use Committee at Tulane University.

Embryos or embryonic hearts were harvested from timed pregnant female mice, fixed in 4% paraformaldehyde (PFA) at 4°C overnight, embedded in paraffin wax and sectioned at 8µm for Hematoxylin and Eosin or immunofluorescent staining, as described previously (Ye et al., 2015b). The primary antibodies used in this study were: anti-Hcn4 (ab32675, Abcam; 1:500), anti-Nkx2-5 (sc-8697, Santa Cruz; 1:500), anti-Tbx3 (sc-17871, Santa Cruz; 1:500), anti-Cx40 (sc-20466, Santa Cruz; 1:250), anti-islet1 (ab20670, Abcam; 1:1000) and anti-GFP (sc-9996, Santa Cruz; 1:500). The secondary antibodies used at 1:1000 dilution and all from Life Technologies were: donkey anti-mouse (A21202, A31571), donkey anti-rat (A21208, A21209), donkey anti-rabbit (A31573) and donkey anti-goat (A32849, A11058, A11055).

In situ hybridization was performed with the RNAscope Intro Pack 2.5 HD Reagent Kit Brown-Mm (Advanced Cell Diagnostics, 322371) according to the manufacturer's instructions. Probe information is as below: *Scn5a* probe (RNAscope Probe - Mm-Scn5a, 429881), *Smoc2* probe (RNAscope Probe-Mm-Smoc2, 318541) and *Acvr1c* probe (RNAscope Probe - Mm-Acvr1c, 429291). All experiments were repeated at least three times.

Surface ECG and whole-cell patch-clamp recordings

Surface ECG recordings of 1-month-old and older mice were conducted as reported previously (Ye et al., 2015b). For *exo utero* ECG recording of developing embryos, timed pregnant females were subjected to *exo utero* surgery as described previously (Song et al., 2008). After the opening of the body wall, the uterus was subsequently opened with iridectomy scissors at the opposite site of the placenta. An incision was then made in the extraembryonic membrane to allow the embryo to emerge but remain attached to the uterus via the placenta. Embryos were then positioned properly with styrofoam within the female abdomen, and ECGs were measured with subcutaneous electrode needles.

The SAN head, SAN junction and adjacent atrial tissue of embryonic hearts from *Shox2*$^{HA\text{-}DsRed}$;*Nkx2.5*$^{Cre/+}$;*R26R*^{YFP} mice at designated age were removed using a fluorescent dissecting microscope. Tissues were dissociated into single cells and were plated onto fibronectin/gelatin-coated coverslips and cultured overnight prior to whole-cell patch-clamp recordings, as described previously (Sun et al., 2015). A coverslip with attached cells was transferred to a recording chamber and perfused with an external solution containing (in mM): 140 NaCl, 5.4 KCl, 1.8 $CaCl_2$, 1 $MgCl_2$, 5.5 glucose and 5 HEPES (pH 7.4), 310-320 mOsm. The temperature during recordings was maintained at 37°C. Cell types (atrial cell, YFP^{+}; SAN head cell, DsRed^{+}; SAN junction cell, DsRed^{+}/YFP^{+}) were determined by fluorescent microscopy (BX51WI, Olympus) through a 40× water-immersion objective and DAGE-MTI camera. Patch-clamp recordings were performed with a Multiclamp 700B amplifier (Molecular Devices). Glass pipettes had open tip resistances of 3-5 MΩ and were filled with an internal solution containing (in mM): 120 K-gluconate, 20 KCl, 10 HEPES, 0.2 EGTA, 4 Mg-ATP, 14 Na_2-phosphocreatine and 0.3 Tris-GPT (pH 7.3), 290 mOsm. Only the myocytes with spontaneous action potentials were recorded under both current-clamp and voltage-clamp modes. Signals were filtered at 4-10 kHz and sampled at 50 kHz. Action potentials were characterized by amplitude, maximal upstroke velocity (dV/dt_{max}), duration at 50% and 90% repolarization (ADP50 and ADP90), the ratio of ADP50 and ADP90, the maximal diastolic potential (MDP), and frequency. Voltage steps were applied to measure different channel-mediated currents.

scRNA-seq

For scRNA-seq, the entire SAN and adjacent atrial tissue, as shown in Fig. 2A, were dissected out from E13.5 *Shox2*$^{Cre/+}$;*R26R*^{mTmG} mice under a stereo fluorescent microscope, subjected to digestion by a cocktail of collagenase I, II and IV, and followed by a brief StemPro Accutase treatment. The suspended cells were processed immediately as follows. Cell count and viability were determined and 5000 cells were loaded for capture onto 10x Genomics Chromium system using single-cell 3′ library and gel bead kit v2. Following capture and lysis, cDNA was synthesized and amplified following the manufacturer's protocol. The amplified cDNAs from each channel of the Chromium System were used to construct an Illumina sequencing library and sequenced on NextSeq 500 with 150 cycle sequencing. Illumina basecall files (*.bcl) were converted to FASTQs using the bcl2fastq2/2.17.1 wrapped in CellRanger/2.1.0. FASTQ files were then aligned to the mm10 mouse reference genome using the CellRanger/2.1.0 software pipeline with default parameters, followed by data analysis in Seurat and Monocle2.

3D reconstruction

For 3D reconstruction, consecutive 10 µm sections were stained using anti-Hcn4 antibodies, imaged, and loaded into Amira 6.0.1, in which subsequent alignment, segmentation, and 3D model generation were performed.

RT-qPCR analyses

For quantitative reverse transcription polymerase chain reaction (RT-qPCR), the SAN was isolated from P0 *Shox2*$^{Cre/+}$;*R26R*^{mTmG} and *Shox2*$^{Cre/+}$;*Nkx2.5*$^{F/F}$;*R26R*^{mTmG} mice (N=3 for each genotype), and subjected to RNA extraction (RNeasy Micro Kit; Qiagen). The RNAs were subsequently reversely transcribed into complementary DNAs (cDNAs) (RevertAid First Strand cDNA Synthesis Kit). SYBR green and gene-specific primers were used and transcript levels were examined using a CFX96 Real-Time PCR Detection System. Primer details are as follows: *Hcn4* (F, 5′-CTTCTGCTGTGTCACTGGGA-3′; R, 5′-ATACTGCTTCC-CCCAGGAGT-3′), *Shox2* (F, 5′-ACCAATTTTACCCTGGAACAAC-3′; R, 5′-TCGATTTTGAAACCAAACCTG-3′), *Nkx2-5* (F, 5′-TTAGGAGAAG-GGCGATGACT-3′; R, 5′-AGGTCCGAGACACCAGGCTA-3′), *Scn5a* (F, 5′-ATGGCAAACTTCCTGTTACCTC-3′; R, 5′-CCACGGGCTTGTTTT-TCAGC-3′), *Isl1* (F, 5′-ATGATGGTGGTTTACAGGCTAAC-3′; R, 5′-TC GATGCTACTTCACTGCCAG-3′), *Gja5* (F, 5′-GGTCCACAAGCACTCC ACAG-3′; R, 5′-CTGAATGGTATCGCACCGGAA-3′), *GAPDH* (F, 5′-A-TCAAGAAGGTGGTGAAGCAG-3′; R, 5′-GAGTGGGAGTTGCTGTT-GAAGT-3′). Differences in the RT-qPCR were analyzed using Student's t-test in GraphPad Prism7; results are presented as mean±s.e.m. P<0.05 was considered significant.

Statistical analysis

To ensure scientific rigor and reproducibility, all experiments were repeated at least three times unless specifically indicated. Quantification results are presented as mean±s.e.m., and statistical analysis was conducted using Student's *t*-test. $P<0.05$ was considered significant.

Acknowledgements

We thank Kejing Song and Alanna Wanek at the NextGen Sequencing Core in the Tulane Center for Translational Research in Infection and Inflammation for technical assistance with scRNA-seq and initial bioinformatic analyses. We also thank Dr Stryder Meadows for reading and editing the manuscript.

Competing interests

The authors declare no competing or financial interests.

Author contributions

Conceptualization: Y.C., H.L., C.-L.C., H.H., Y.Z.; Methodology: Y.C., H.L.; Software: H.L., Z.H., Q.T.; Validation: Y.C., H.L.; Formal analysis: H.L., D.L., Z.H., Q.T.; Investigation: H.L., D.L., Y.W., J.X., T.Y., L.W.; Resources: Y.C., C.-L.C.; Data curation: Y.C., H.L., D.L.; Writing - original draft: H.L., Y.W., Q.T.; Writing - review & editing: Y.C., C.-L.C., H.H., Y.Z.; Visualization: H.L.; Supervision: Y.C.; Project administration: Y.C.; Funding acquisition: Y.C.

Funding

We acknowledge financial support from the National Institutes of Health (R01HL136326 to Y.C.). H.H. is supported by the National Institutes of Health (R01DC016324). H.L. was supported in part by a fellowship from Fujian Normal University, and J.X. and L.W. received fellowship from the China Scholarship Council. Deposited in PMC for release after 12 months.

Data availability

scRNA-Seq data have been deposited in GEO under accession number GSE130461.

Supplementary information

Supplementary information available online at
http://dev.biologists.org/lookup/doi/10.1242/dev.178145.supplemental

References

Barry, D. M., Xu, K., Meadows, S. M., Zheng, Y., Norden, P. R., Davis, G. E. and Cleaver, O. (2015). Cdc42 is required for cytoskeletal support of endothelial cell adhesion during blood vessel formation in mice. *Development* **142**, 3058-3070. doi:10.1242/dev.125260

Benson, D. W., Silberbach, G. M., Kavanaugh-McHugh, A., Cottrill, C., Zhang, Y., Riggs, S., Smalls, O., Johnson, M. C., Watson, M. S. and Seidman, J. (1999). Mutations in the cardiac transcription factor NKX2. 5 affect diverse cardiac developmental pathways. *J. Clin. Invest.* **104**, 1567-1573. doi:10.1172/JCI8154

Biben, C., Weber, R., Kesteven, S., Stanley, E., McDonald, L., Elliott, D. A., Barnett, L., KÖentgen, F., Robb, L. and Feneley, M. (2000). Cardiac septal and valvular dysmorphogenesis in mice heterozygous for mutations in the homeobox gene Nkx2-5. *Circ. Res.* **87**, 888-895. doi:10.1161/01.RES.87.10.888

Blaschke, R. J., Hahurij, N. D., Kuijper, S., Just, S., Wisse, L. J., Deissler, K., Maxelon, T. and Anastassiadis, K. (2007). Targeted mutation reveals essential functions of the homeodomain transcription factor Shox2 in sinoatrial and pacemaking development. *Circulation* **115**, 1830-1838. doi:10.1161/CIRCULATIONAHA.106.637819

Boyett, M. R., Honjo, H. and Kodama, I. (2000). The sinoatrial node, a heterogeneous pacemaker structure. *Cardiovasc. Res.* **47**, 658-687. doi:10.1016/S0008-6363(00)00135-8

Butler, A., Hoffman, P., Smibert, P., Papalexi, E. and Satija, R. (2018). Integrating single-cell transcriptomic data across different conditions, technologies, and species. *Nat. Biotechnol.* **36**, 411-420. doi:10.1038/nbt.4096

Chasseigneaux, S., Moraca, Y., Cochois-Guégan, V., Boulay, A.-C., Gilbert, A., Le Crom, S., Blugeon, C., Firmo, C., Cisternino, S. and Laplanche, J.-L. (2018). Isolation and differential transcriptome of vascular smooth muscle cells and mid-capillary pericytes from the rat brain. *Sci. Rep.* **8**, 12272. doi:10.1038/s41598-018-30739-5

Christoffels, V. M., Mommersteeg, M. T., Trowe, M.-O., Prall, O. W., de Gier-de Vries, C., Soufan, A. T., Bussen, M., Schuster-Gossler, K., Harvey, R. P. and Moorman, A. F. (2006). Formation of the venous pole of the heart from an Nkx2-5-negative precursor population requires Tbx18. *Circ. Res.* **98**, 1555-1563. doi:10.1161/01.RES.0000227571.84189.65

Christoffels, V. M., Smits, G. J., Kispert, A. and Moorman, A. F. M. (2010). Development of the pacemaker tissues of the heart. *Circ. Res.* **106**, 240-254. doi:10.1161/CIRCRESAHA.109.205419

DeLaughter, D. M., Bick, A. G., Wakimoto, H., McKean, D., Gorham, J. M., Kathiriya, I. S., Hinson, J. T., Homsy, J., Gray, J. and Pu, W. (2016). Single-cell resolution of temporal gene expression during heart development. *Dev. Cell* **39**, 480-490. doi:10.1016/j.devcel.2016.10.001

Espinoza-Lewis, R. A., Yu, L., He, F., Liu, H., Tang, R., Shi, J., Sun, X., Martin, J. F., Wang, D. and Yang, J. (2009). Shox2 is essential for the differentiation of cardiac pacemaker cells by repressing Nkx2-5. *Dev. Biol.* **327**, 376-385. doi:10.1016/j.ydbio.2008.12.028

Espinoza-Lewis, R. A., Liu, H., Sun, C., Chen, C., Jiao, K. and Chen, Y. (2011). Ectopic expression of Nkx2. 5 suppresses the formation of the sinoatrial node in mice. *Dev. Biol.* **356**, 359-369. doi:10.1016/j.ydbio.2011.05.663

Jay, P. Y., Harris, B. S., Maguire, C. T., Buerger, A., Wakimoto, H., Tanaka, M., Kupershmidt, S., Roden, D. M., Schultheiss, T. M. and O'Brien, T. X. (2004). Nkx2-5 mutation causes anatomic hypoplasia of the cardiac conduction system. *J. Clin. Invest.* **113**, 1130-1137. doi:10.1172/JCI19846

Joyner, R. W. and Van Capelle, F. (1986). Propagation through electrically coupled cells. How a small SA node drives a large atrium. *Biophys. J.* **50**, 1157-1164. doi:10.1016/s0006-3495(86)83559-7

Kasahara, H., Bartunkova, S., Schinke, M., Tanaka, M. and Izumo, S. (1998). Cardiac and extracardiac expression of Csx/Nkx2. 5 homeodomain protein. *Circ. Res.* **82**, 936-946. doi:10.1161/01.RES.82.9.936

Khazen, W., M'Bika, J.-P., Tomkiewicz, C., Benelli, C., Chany, C., Achour, A. and Forest, C. (2005). Expression of macrophage-selective markers in human and rodent adipocytes. *FEBS Lett.* **579**, 5631-5634. doi:10.1016/j.febslet.2005.09.032

Lee, J. H., Protze, S. I., Laksman, Z., Backx, P. H. and Keller, G. M. (2017). Human pluripotent stem cell-derived atrial and ventricular cardiomyocytes develop from distinct mesoderm populations. *Cell Stem Cell* **21**, 179-194.e4. doi:10.1016/j.stem.2017.07.003

Li, G., Xu, A., Sim, S., Priest, J. R., Tian, X., Khan, T., Quertermous, T., Zhou, B., Tsao, P. S. and Quake, S. R. (2016). Transcriptomic profiling maps anatomically patterned subpopulations among single embryonic cardiac cells. *Dev. Cell* **39**, 491-507. doi:10.1016/j.devcel.2016.10.014

Liang, X., Wang, G., Lin, L., Lowe, J., Zhang, Q., Bu, L., Chen, Y., Chen, J., Sun, Y. and Evans, S. M. (2013). HCN4 dynamically marks the first heart field and conduction system precursors. *Circ. Res.* **113**, 399-407. doi:10.1161/CIRCRESAHA.113.301588

Liang, X., Zhang, Q., Cattaneo, P., Zhuang, S., Gong, X., Spann, N. J., Jiang, C., Cao, X., Zhao, X. and Zhang, X. (2015). Transcription factor ISL1 is essential for pacemaker development and function. *J. Clin. Invest.* **125**, 3256-3268. doi:10.1172/JCI68257

Lints, T. J., Parsons, L. M., Hartley, L., Lyons, I. and Harvey, R. P. (1993). Nkx-2.5: a novel murine homeobox gene expressed in early heart progenitor cells and their myogenic descendants. *Development* **119**, 419-431.

Liu, J., Dobrzynski, H., Yanni, J., Boyett, M. R. and Lei, M. (2007). Organisation of the mouse sinoatrial node: structure and expression of HCN channels. *Cardiovasc. Res.* **73**, 729-738. doi:10.1016/j.cardiores.2006.11.016

Maaten, L. v. d. and Hinton, G. (2008). Visualizing data using t-SNE. *J. Mach. Learn. Res.* **9**, 2579-2605.

MacLean, W., Karp, R. B., KouCHOUKOS, N. T., James, T. N. and Waldo, A. L. (1975). P waves during ectopic atrial rhythms in man: a study utilizing atrial pacing with fixed electrodes. *Circulation* **52**, 426-434. doi:10.1161/01.CIR.52.3.426

Macosko, E. Z., Basu, A., Satija, R., Nemesh, J., Shekhar, K., Goldman, M., Tirosh, I., Bialas, A. R., Kamitaki, N. and Martersteck, E. M. (2015). Highly parallel genome-wide expression profiling of individual cells using nanoliter droplets. *Cell* **161**, 1202-1214. doi:10.1016/j.cell.2015.05.002

Mommersteeg, M. T. M., Hoogaars, W. M. H., Prall, O. W., de Gier-de Vries, C., Wiese, C., Clout, D. E. W., Papaioannou, V. E., Brown, N. A., Harvey, R. P. and Moorman, A. F. M. (2007). Molecular pathway for the localized formation of the sinoatrial node. *Circ. Res.* **100**, 354-362. doi:10.1161/01.RES.0000258019.74591.b3

Moorman, A. F. M., de Jong, F., Denyn, M. M. F. J. and Lamers, W. H. (1998). Development of the cardiac conduction system. *Circ. Res.* **82**, 629-644. doi:10.1161/01.RES.82.6.629

Moosmang, S., Stieber, J., Zong, X., Biel, M., Hofmann, F. and Ludwig, A. (2001). Cellular expression and functional characterization of four hyperpolarization-activated pacemaker channels in cardiac and neuronal tissues. *Eur. J. Biochem.* **268**, 1646-1652. doi:10.1046/j.1432-1327.2001.02036.x

Moses, K. A., DeMayo, F., Braun, R. M., Reecy, J. L. and Schwartz, R. J. (2001). Embryonic expression of an Nkx2-5/Cre gene using ROSA26 reporter mice. *Genesis* **31**, 176-180. doi:10.1002/gene.10022

Munshi, N. V. (2012). Gene regulatory networks in cardiac conduction system development. *Circ. Res.* **110**, 1525-1537. doi:10.1161/CIRCRESAHA.111.260026

Muzumdar, M. D., Tasic, B., Miyamichi, K., Li, L. and Luo, L. (2007). A global double-fluorescent Cre reporter mouse. *Genesis* **45**, 593-605. doi:10.1002/dvg.20335

Opthof, T. (1988). The mammalian sinoatrial node. *Cardiovasc. Drugs Ther.* **1**, 573-597. doi:10.1007/BF02125744

Pashmforoush, M., Lu, J. T., Chen, H., St Amand, T., Kondo, R., Pradervand, S., Evans, S. M., Clark, B., Feramisco, J. R. and Giles, W. (2004). Nkx2-5 pathways

and congenital heart disease: loss of ventricular myocyte lineage specification leads to progressive cardiomyopathy and complete heart block. *Cell* **117**, 373-386. doi:10.1016/S0092-8674(04)00405-2

Puskaric, S., Schmitteckert, S., Mori, A. D., Glaser, A., Schneider, K. U., Bruneau, B. G., Blaschke, R. J., Steinbeisser, H. and Rappold, G. (2010). Shox2 mediates Tbx5 activity by regulating Bmp4 in the pacemaker region of the developing heart. *Hum. Mol. Genet.* **19**, 4625-4633. doi:10.1093/hmg/ddq393

Qiu, X., Mao, Q., Tang, Y., Wang, L., Chawla, R., Pliner, H. A. and Trapnell, C. (2017). Reversed graph embedding resolves complex single-cell trajectories. *Nat. Methods* **14**, 979-982. doi:10.1038/nmeth.4402

Santoro, B. and Tibbs, G. R. (1999). The HCN gene family: molecular basis of the hyperpolarization-activated pacemaker channels. *Ann. N. Y. Acad. Sci.* **868**, 741-764. doi:10.1111/j.1749-6632.1999.tb11353.x

Schott, J.-J., Benson, D. W., Basson, C. T., Pease, W., Silberbach, G. M., Moak, J. P., Maron, B. J., Seidman, C. E. and Seidman, J. G. (1998). Congenital heart disease caused by mutations in the transcription factor NKX2-5. *Science* **281**, 108-111. doi:10.1126/science.281.5373.108

Song, Y., Yan, M., Muneoka, K. and Chen, Y. P. (2008). Mouse embryonic diastema region is an ideal site for the development of ectopically transplanted tooth germ. *Dev. Dyn.* **237**, 411-416. doi:10.1002/dvdy.21427

Souders, C. A., Bowers, S. L. K. and Baudino, T. A. (2009). Cardiac fibroblast: the renaissance cell. *Circ. Res.* **105**, 1164-1176. doi:10.1161/CIRCRESAHA.109.209809

Sun, C., Zhang, T., Liu, C., Gu, S. and Chen, Y. P. (2013). Generation of Shox2-Cre allele for tissue specific manipulation of genes in the developing heart, palate, and limb. *Genesis* **51**, 515-522. doi:10.1002/dvg.22397

Sun, C., Yu, D., Ye, W., Liu, C., Gu, S., Sinsheimer, N. R., Song, Z., Li, X., Chen, C., Song, Y. et al. (2015). The short stature homeobox 2 (Shox2)-bone morphogenetic protein (BMP) pathway regulates dorsal mesenchymal protrusion development and its temporary function as a pacemaker during cardiogenesis. *J. Biol. Chem.* **290**, 2007-2023. doi:10.1074/jbc.M114.619007

Tan, D. W. B., Jensen, K. B., Trotter, M. W., Connelly, J. T., Broad, S. and Watt, F. M. (2013). Single-cell gene expression profiling reveals functional heterogeneity of undifferentiated human epidermal cells. *Development* **140**, 1433-1444. doi:10.1242/dev.087551

Tarnawski, L., Xian, X., Monnerat, G., Macaulay, I. C., Malan, D., Borgman, A., Wu, S. M., Fleischmann, B. K. and Jovinge, S. (2015). Integrin based isolation enables purification of murine lineage committed cardiomyocytes. *PLoS ONE* **10**, e0135880. doi:10.1371/journal.pone.0135880

van Eif, V. W. W., Stefanovic, S., van Duijvenboden, K., Bakker, M., Wakker, V., de Gier-de Vries, C., Zaffran, S., Verkerk, A. O., Boukens, B. J. and Christoffels, V. M. (2019). Transcriptome analysis of mouse and human sinoatrial node cells reveals a conserved genetic program. *Development* **146**, dev173161. doi:10.1242/dev.173161

Vanlandewijck, M., He, L., Mäe, M. A., Andrae, J., Ando, K., Del Gaudio, F., Nahar, K., Lebouvier, T., Laviña, B. and Gouveia, L. (2018). A molecular atlas of cell types and zonation in the brain vasculature. *Nature* **554**, 475-480. doi:10.1038/nature25739

van Weerd, J. H. and Christoffels, V. M. (2016). The formation and function of the cardiac conduction system. *Development* **143**, 197-210. doi:10.1242/dev.124883

Vedantham, V., Galang, G., Evangelista, M., Deo, R. C. and Srivastava, D. (2015). RNA sequencing of mouse sinoatrial node reveals an upstream regulatory role for Islet-1 in cardiac pacemaker cells. *Circ. Res.* **116**, 797-803. doi:10.1161/CIRCRESAHA.116.305913

Verheijck, E. E., Wessels, A., van Ginneken, A. C., Bourier, J., Markman, M. W. M., Vermeulen, J. L. M., de Bakker, J. M. T., Lamers, W. H., Opthof, T. and Bouman, L. N. (1998). Distribution of atrial and nodal cells within the rabbit sinoatrial node: models of sinoatrial transition. *Circulation* **97**, 1623-1631. doi:10.1161/01.CIR.97.16.1623

Wiese, C., Grieskamp, T., Airik, R., Mommersteeg, M. T. M., Gardiwal, A., de Gier-de Vries, C., Schuster-Gossler, K., Moorman, A. F. M., Kispert, A. and Christoffels, V. M. (2009). Formation of the sinus node head and differentiation of sinus node myocardium are independently regulated by Tbx18 and Tbx3. *Circ. Res.* **104**, 388-397. doi:10.1161/CIRCRESAHA.108.187062

Wu, M., Peng, S., Yang, J., Tu, Z., Cai, X., Cai, C.-L., Wang, Z. and Zhao, Y. (2014). Baf250a orchestrates an epigenetic pathway to repress the Nkx2.5-directed contractile cardiomyocyte program in the sinoatrial node. *Cell Res.* **24**, 1201-1213. doi:10.1038/cr.2014.113

Ye, W., Song, Y., Huang, Z., Zhang, Y. and Chen, Y. (2015a). Genetic regulation of sinoatrial node development and pacemaker program in the venous pole. *J. Cardiovasc. Dev. Dis.* **2**, 282-298. doi:10.3390/jcdd2040282

Ye, W., Wang, J., Song, Y., Yu, D., Sun, C., Liu, C., Chen, F., Zhang, Y., Wang, F., Harvey, R. P. et al. (2015b). A common Shox2-Nkx2-5 antagonistic mechanism primes the pacemaker cell fate in the pulmonary vein myocardium and sinoatrial node. *Development* **142**, 2521-2532. doi:10.1242/dev.120220

Zhang, H., Holden, A. V. and Boyett, M. R. (2001). Gradient model versus mosaic model of the sinoatrial node. *Circulation* **103**, 584-588. doi:10.1161/01.CIR.103.4.584

Zhang, Y. M., Hartzell, C., Narlow, M. and Dudley, S. C., Jr (2002). Stem cell-derived cardiomyocytes demonstrate arrhythmic potential. *Circulation* **106**, 1294-1299. doi:10.1161/01.CIR.0000027585.05868.67

Supplementary Materials

Supplemental Figures

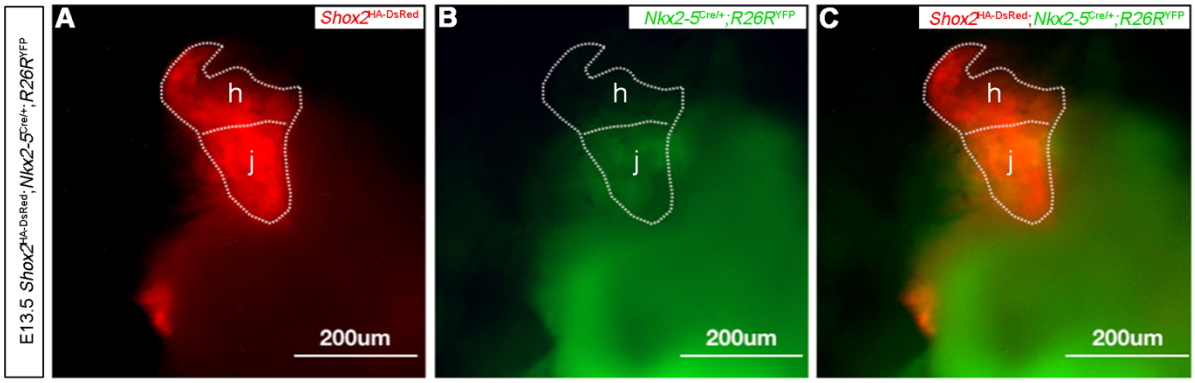

Figure S1

Figure S1. Colocalization of YFP and DsRed in the SAN junction of *Shox2*$^{HA\text{-}DsRed}$;*Nkx2-5*$^{Cre/+}$;*R26R*^{YFP} mice.

(A-C) Visualization of the heart of an E13.5 *Shox2*$^{HA\text{-}DsRed}$;*Nkx2-5*$^{Cre/+}$;*R26R*^{YFP} mouse under fluorescent stereomicroscope reveals colocalization of YFP and DsRed in the SAN junction. h, SAN head; j, SAN junction.

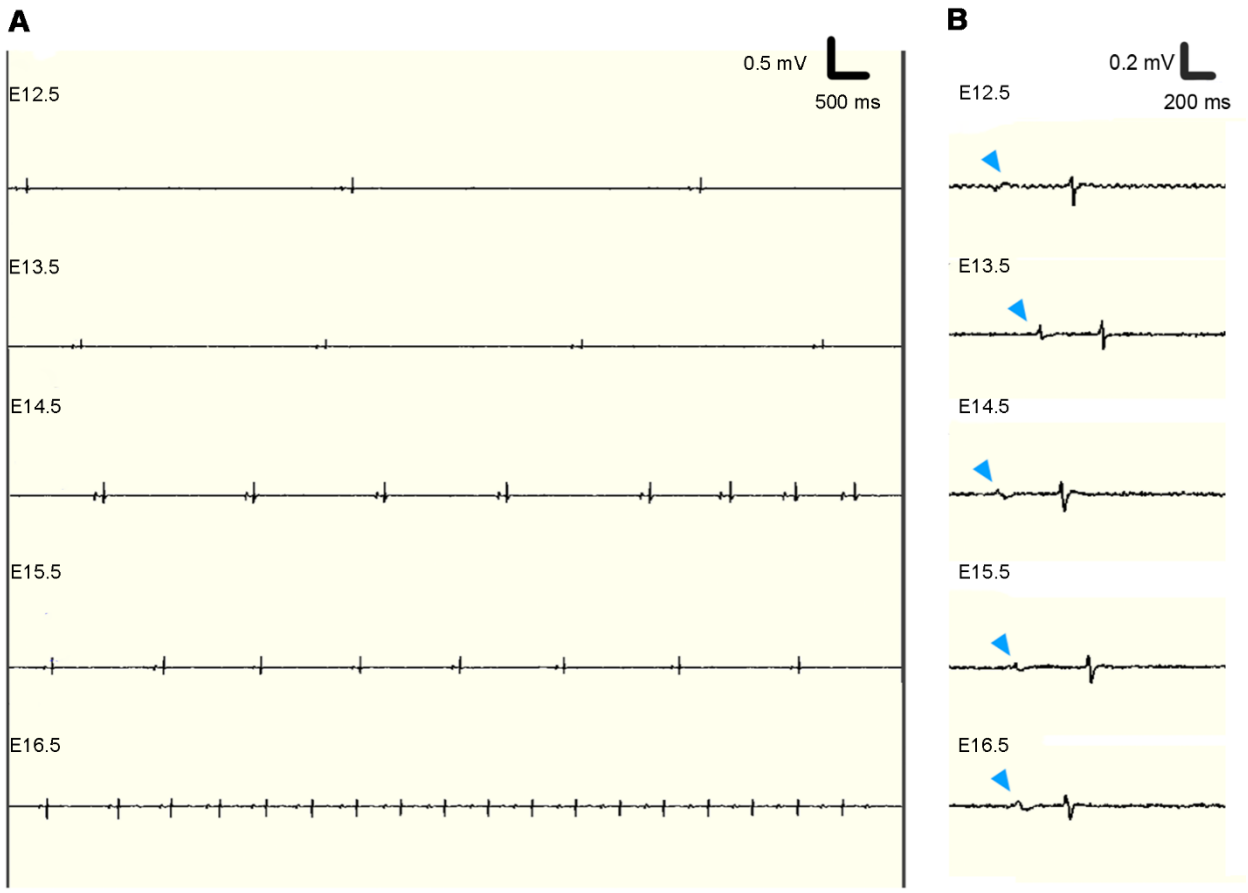

Figure S2

Figure S2. ECG recordings on developing mouse embryos.

(A) Representative ECG recordings of lead II on the embryos at E12.5, E13.5, E14.5, E15.5 and E16.5, respectively. (B) Representative single PQRS compress recordings on the embryos at different stage. Blue arrowheads point to P wave.

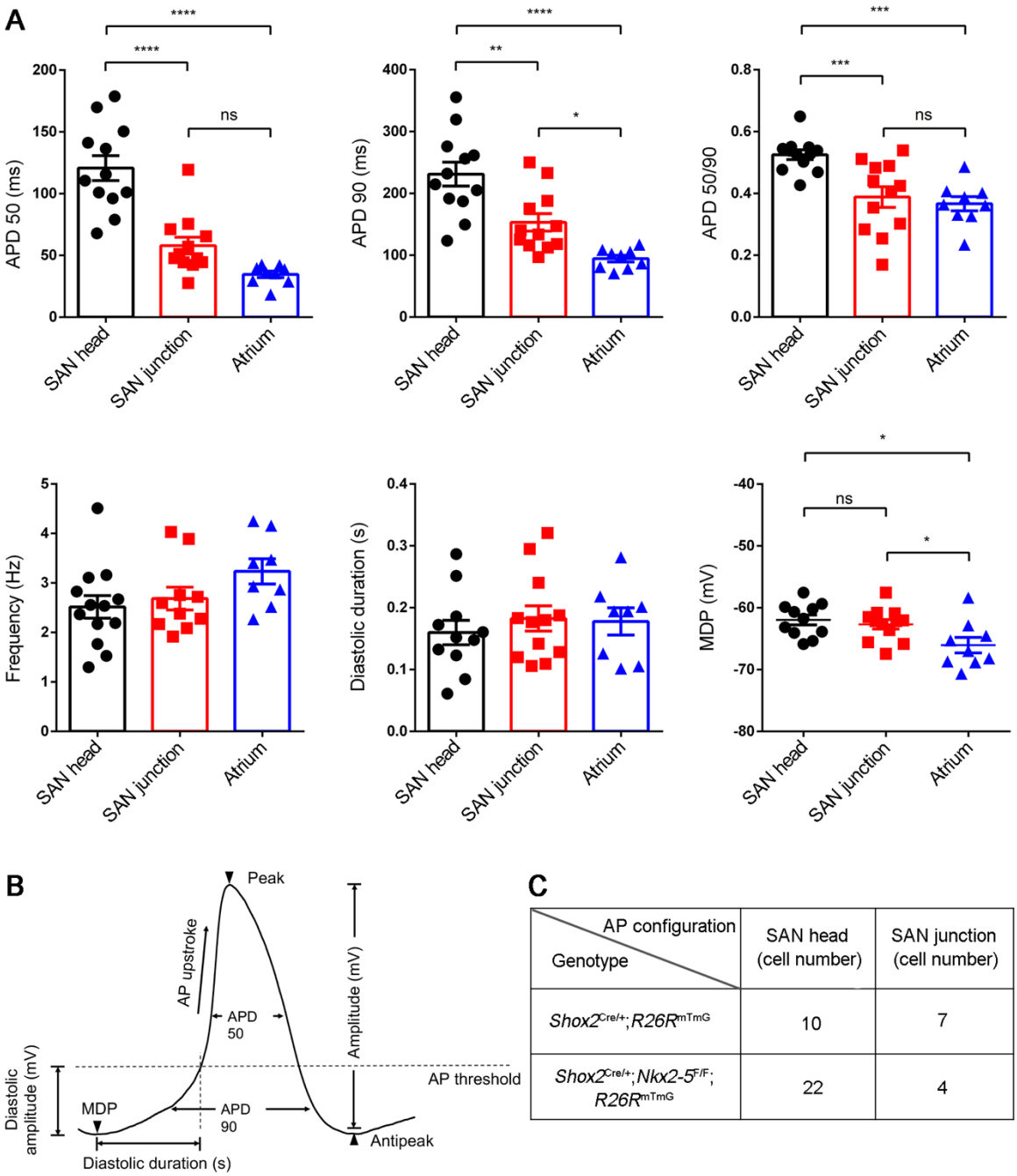

C

AP configuration / Genotype	SAN head (cell number)	SAN junction (cell number)
Shox2$^{Cre/+}$;*R26R*^{mTmG}	10	7
Shox2$^{Cre/+}$;*Nkx2-5*$^{F/F}$;*R26R*^{mTmG}	22	4

Figure S3

Figure S3. Comparison of the AP parameters between the SAN head, SAN junction, and atrial myocardial cells.

(A, B) Histograms show AP parameters of the SAN head, SAN junction, and atrial myocardial cells at E13.5. (C) A table summarizing cell numbers exhibiting the SAN head and SAN junction AP configurations, respectively, by patch clamp recording on GFP-positive cells

isolated from the SAN of E13.5 *Shox2*$^{Cre/+}$;*R26R*^{mTmG} and *Shox2*$^{Cre/+}$;*Nkx2-5*$^{F/F}$;*R26R*^{mTmG} mice.

ns, non-significant; *, $p<0.05$; **, $p<0.01$; ***, $p<0.001$; ****, $p<0.0001$.

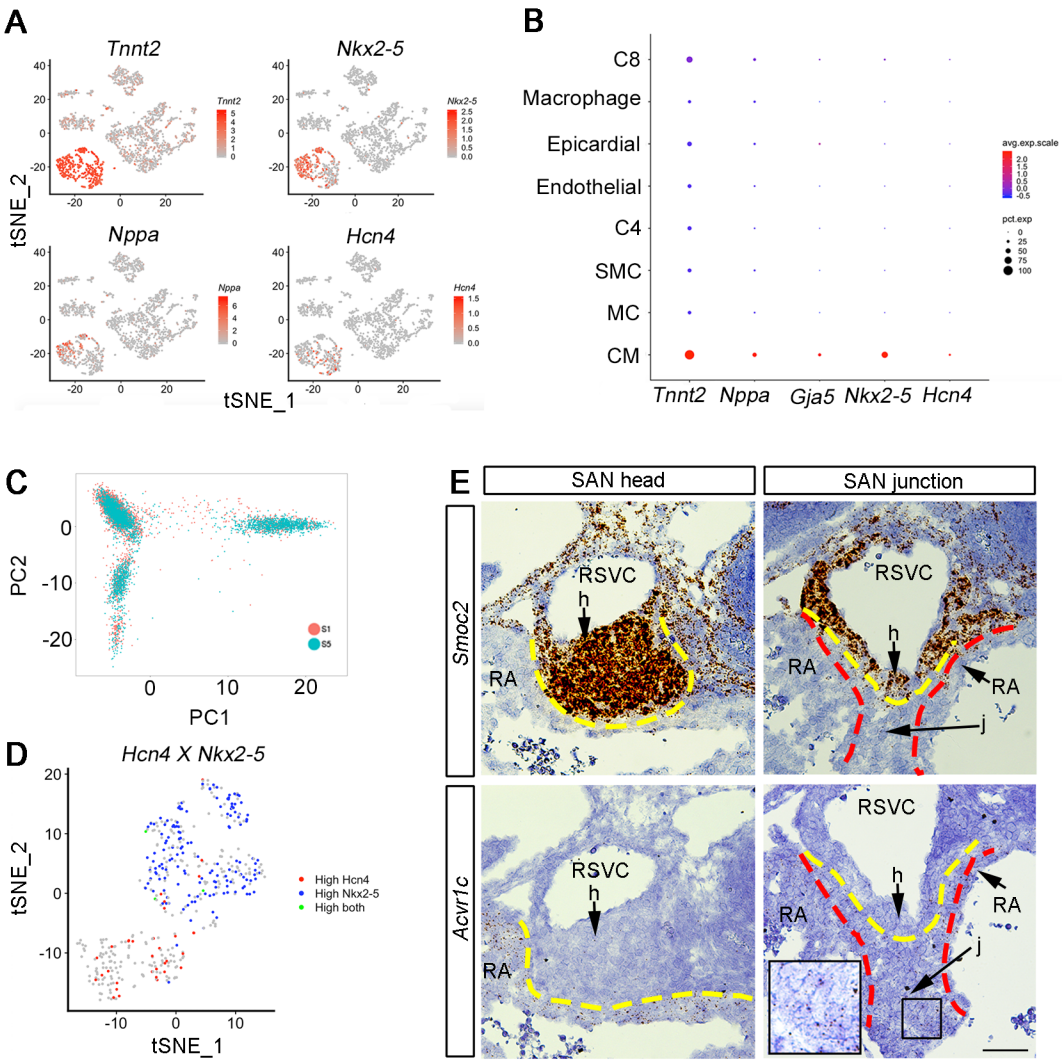

Figure S4

Figure S4. Quality control and cell selection for deeper scRNA-seq data analysis.

(A, B) The expression of *Tnnt2*, *Hcn4*, *Nkx2-5*, *Gja5* and *Nppa* within the CM cluster is visualized by FeaturePlot (A) and DotPlot (B). (C) PCAPlot on S1 and S5 shows the high coincidence between them. (D) FeaturePlot shows the co-expression of *Hcn4* and *Nkx2-5* within different clusters. (E) *In situ* hybridization shows specific *Smoc2* expression in the SAN head and *Acvr1c* expression in the SAN junction and atrial cells at E13.5 wild type embryo, respectively. h, SAN head; j, SAN junction; CM, cardiomyocyte; EC, endothelial cells; MC, mesenchymal cells; RA, right atrium; EPI, epicardial cells; SMC, smooth muscle cells; RSVC, right superior vena cava. C4, C8, cluster number 4, 8. Bar: 50 μm.

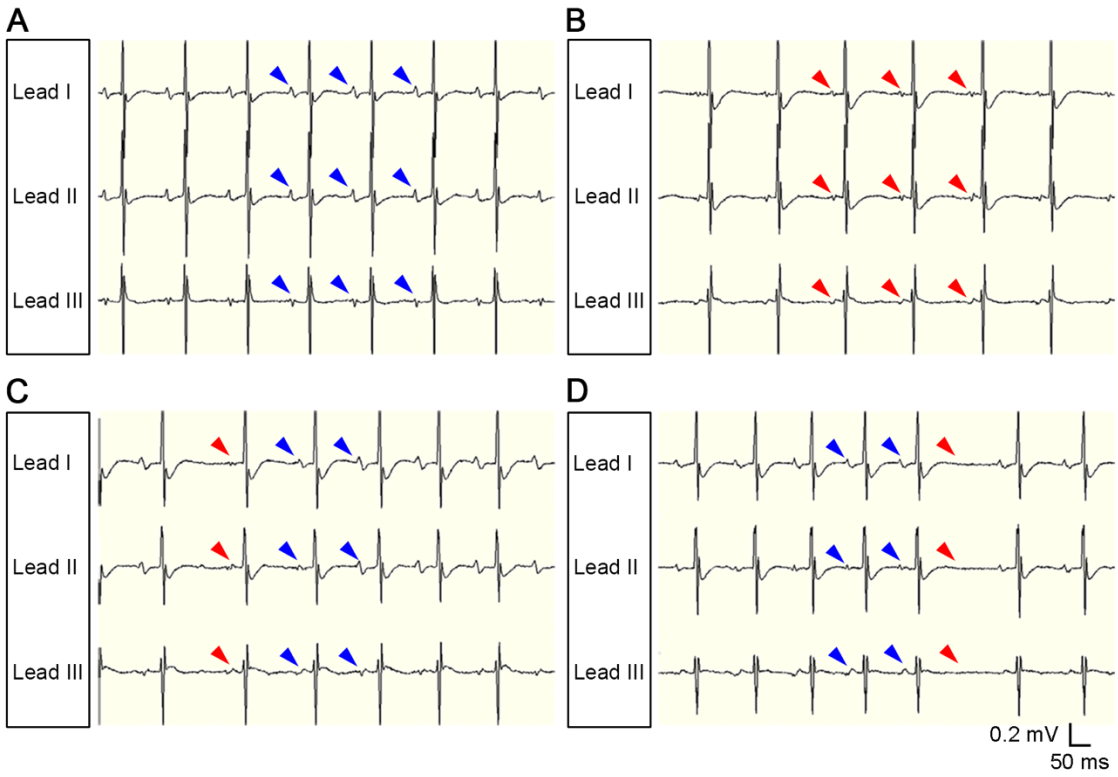

Figure S5

Figure S5. Closer looks at the surface ECG records on *Shox2*$^{Cre/+}$;*Nkx2-5*$^{F/F}$ mice

(A-D) Typical examples of surface ECG recordings (lead I, lead II and lead III) of the adult *Shox2*$^{Cre/+}$;*Nkx2-5*$^{F/F}$ mice. Blue arrowheads point to normal P wave. Red arrowheads point to abnormal P wave.